LAETITIA MACÉ, LAURENT SOUCHE and JEAN-LAURENT MALLET, Gocad Research Group, Nancy, France.

3D Fracture Modeling Integrating Geomechanics and Geologic Data.

1 Introduction

Natural fractures have dramatic effects on reservoirs in term of oil recovery, because they often control the hydraulic flow as conductors (open fractures) or barriers (mineralized fractures). Predicting the performance of fractured reservoirs requires the characterization of all fracture parameters such as spacing, orientation, size and aperture. However, none of these fracture attributes is typically well constrained by available subsurface data either because of the restricted number and size of samples (wellbores) or because of the indirectness of measurements (seismic). In [12], Ouenes uses neural networks to identify fracture key parameters, whereas Bourne in [4] proposes to integrate geomechanics in fracture characterization. Another common technique used to predict fracture characteristics is the computation of curvatures (see [13]), however this parameter often appears to be loosely correlated with the presence of fractures.

Fractures initiation and propagation are mainly due to lithology and local stress distribution (see [10]). In our approach, geologic observations and rock mechanical properties are combined with a fracture geomechanics-based model to predict fracture network attributes. Although the stress field history may only be known after long studies of the field by experts (e.g. regional stress history in [4]), the global stress field can be evaluated through the knowledge of the strain tensor. Then, based on assumptions on the values of mechanical rock properties (cohesion, Young's modulus, etc.) and on their uncertainties, a probability of fracturation is computed through the model. Moreover, combined with other fracture drivers and calibrated with well data, this new fracture parameter enables to determine a fracture density analogue. The other fracture attributes (size, orientation) are characterized through 3D distribution laws obtained from mechanical analysis and well data. Discrete Fracture Networks (DFNs) are finally generated using the previously computed fracture attributes and a heterogeneous Poisson point process.

First, a new approach of fracture characterization including geological uncertainties is described. Then, the stochastic generation of DFNs from 3D fracture attributes is detailed. Methods for assessing equivalent fracture permeability are finally discussed.

2 Fracture characterization

Strains and Stresses

Fractures form when rock cannot withstand the in-situ stress anymore and their orientation is constrained by the direction of principal stresses. Fracturation patterns thus highly depend on stress history which is itself related to strain history. The 3D Strain Tensor can be obtained at any point in the subsurface through two different methods :

- 3D balanced unfolding of layers (see [8]),
- evaluation of the total deformations in the "Geo-Chronological space" from deposition time to present (see [9]).

Moreover, assumptions on mechanical elastic properties (the "Lamé" coefficients) characterizing the material (e.g., see [5] and [7]) and on their uncertainties can be represented as probability laws.

If the material is homogeneous, elastic and isotropic, then, according to the generalized Hooke's law, the Lagrangian Strain Tensor $[\mathcal{E}(\mathbf{x})]$ and the Stress Tensor $[\sigma(\mathbf{x})]$ are linked by the following linear equation where $tr([\mathcal{E}(\mathbf{x})])$ represents the trace of $[\mathcal{E}(\mathbf{x})]$ while λ and μ are the so called "Lamé" coefficients at location $\mathbf{x}$:

$$[\sigma(\mathbf{x})] \quad = \quad \lambda \cdot tr([\mathcal{E}(\mathbf{x})]) \cdot [I] \; + \; 2\mu \cdot [\mathcal{E}(\mathbf{x})] \tag{1}$$

In Hooke's law, elongations are counted negatively while contractions are counted positively. So for the consistency of the law, the Lagrangian Strain Tensor must be used in equation (1).

The eigen values $\{\mathcal{E}_1(\mathbf{x}), \mathcal{E}_2(\mathbf{x}), \mathcal{E}_3(\mathbf{x})\}$ of $[\mathcal{E}(\mathbf{x})]$ sorted by increasing magnitude order and their associated eigen vectors $\{\mathbf{W}_1(\mathbf{x}), \mathbf{W}_2(\mathbf{x}), \mathbf{W}_3(\mathbf{x})\}$ are called the Principal Strains and Principal Strain Directions at location $\mathbf{x}$, respectively. Equation (1) also implies that $[\sigma(\mathbf{x})]$ and $[\mathcal{E}(\mathbf{x})]$ must have the same eigen vectors and the same eigen values. The eigen values of $[\sigma(\mathbf{x})]$ and their associated eigen vectors are called, respectively, the Principal Stresses $\{\sigma_i(\mathbf{x})\}$ and the Principal Stress Directions $\{\mathbf{W}_i(\mathbf{x})\}$, where $\mathbf{W}_i$ is also the i^{th} eigen vector of $[\mathcal{E}(\mathbf{x})]$. Still according to the Hooke's law (1), the Principal Strains $\{\mathcal{E}_i(\mathbf{x})\}$ and the Principal Stresses $\{\sigma_i(\mathbf{x})\}$ are linked by the following equation :

$$\sigma_i(\mathbf{x}) \; = \; \lambda \cdot \big(\mathcal{E}_1(\mathbf{x}) + \mathcal{E}_2(\mathbf{x}) + \mathcal{E}_3(\mathbf{x})\big) \; + \; 2\mu \cdot \mathcal{E}_i(\mathbf{x}) \qquad \forall\, i \in \{1,2,3\} \tag{2}$$

Failure criterion

Many criteria exist to predict failure of brittle materials. The *Mohr-Coulomb criterion* is appropriate to model shear fractures whereas the *Griffith criterion* is more appropriate in case of tensile failure. This paper focuses on shear failure.

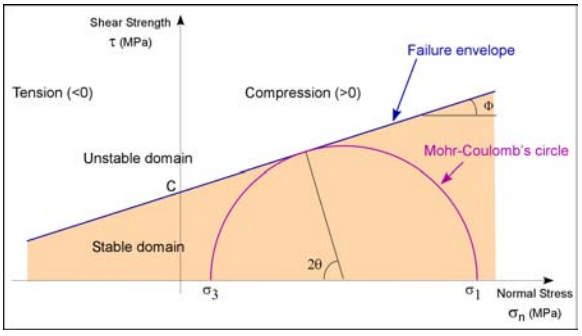

Figure 1: *Mohr-Coulomb's failure criterion. Failure occurs when the Mohr-Coulomb's circle exceeds the failure envelope.*

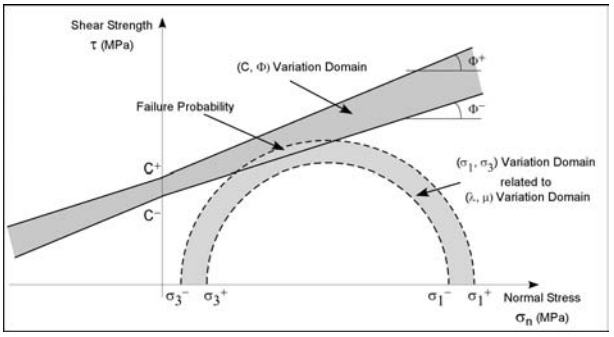

Figure 2: *Mohr-Coulomb's failure criterion including uncertainties on the rock properties C, ϕ, λ and μ considered as Uniform probability laws.*

The Mohr-Coulomb theory assumes that, for the Principal Stresses such that $\sigma_1 > \sigma_2 > \sigma_3$, the intermediate principal stress component σ_2 does not act for the failure. The Mohr-Coulomb theory states that failure occurs when the Mohr-Coulomb's circle at a point in the subsurface exceeds the failure envelope (see [2]). As shown by figure (1), using geometric terms and defining c as the intern cohesion and φ as the rock friction angle, failure occurs when the distance between the center of the Mohr-Coulomb's circle and the failure envelope is smaller than the radius of the Mohr-Coulomb's circle :

$$\frac{\sigma_1 - \sigma_3}{2} \geq \left| \frac{\tan\varphi \; \cdot \; (\frac{\sigma_1+\sigma_3}{2}) \; + \; c}{\sqrt{\tan^2\varphi + 1}} \right| \tag{3}$$

From failure probability...

In practice, the properties $\{\lambda, \mu, c, \varphi\}$ of the material at a given location in the subsurface are not known with precision. So, property uncertainties can be represented as distribution laws respectively $L(\omega)$,

$M(\omega)$, $C(\omega)$ and $\phi(\omega)$. As a consequence, to characterize the fracturation in the subsurface, we propose to integrate these uncertainties through a stochastic model based on equations (2) and (3) (see also figure (2) when probability laws of all rock properties are Uniform). Failure can now be considered as a random event and it makes sense trying to evaluate its probability $PF_{CLM\phi}(\mathcal{E})$ to occur when $\mathcal{E}$ is known and the probability laws of $C(\omega)$, $L(\omega)$, $M(\omega)$ and $\phi(\omega)$ are given :

$$PF_{CLM\phi}(\mathcal{E}) \;=\; I\!P\big(\,\{\omega \in \Omega \;:\; \text{fracturation occurs}\}\,\big) \quad \text{where } (\Omega, \mathcal{A}, I\!P) \text{ is a probabilized space.} \qquad (4)$$

The development of equation (4) leads to resolve integrals. In practice, the kernel of these integrals is not convenient to integrate analytically and the use of numerical integration techniques is far more practical to evaluate the failure probability. On figure (3), the structure of the test case of Split Mountain (Utah) is exaggerated in order to identify its anticlinal structure. Figure (4) shows the Failure Probability computed on this case study when all probability laws of the rock properties are considered to be Gaussian.

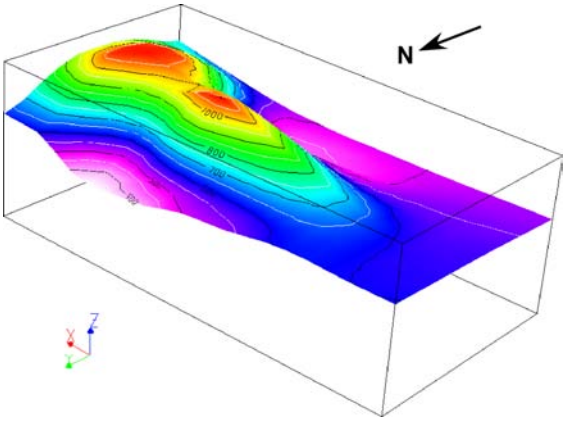

Figure 3: *Split Mountain structure (Utah) composed of a major anticline E-W and a minor one N-S (vertical scale x6). The displayed property is the altitude.*

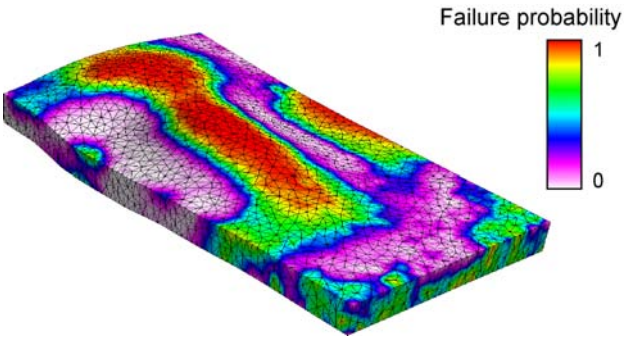

Figure 4: *Tetrahedralized solid of the Split Mountain anticline (Utah) showing the failure probability computed from Gaussian distribution laws on material properties and principal strain values.*

...to fracture density assessment

Using a non-linear multi-regression, the failure probability previously computed is combined with other fracture drivers, such as seismic attributes and layer thickness, in order to obtain a fracture density analogue that reproduces as well as possible observed well data. Mechanical analysis and well data also provide 3D distribution laws of fracture size and orientation, which are used to generate DFNs.

3 Stochastic simulation of DFNs

Each geometric parameter characterizing the fracture networks (spacing, orientation, size) is described by a distribution law which type (e.g. uniform, gaussian) is assumed to be constant over the volume of interest but which characteristic parameters may vary locally. The previous section has provided us with a 3D structured grid painted with these parameters. Aperture and permeability of fractures will not be studied here.

Fracture location

In a homogeneous media, fractures are assumed to be purely randomly distributed (see [10]). At first sight a Poisson process can then describe the spatial distribution of fractures. In [1] a unique parameter, the average fracture density in space, controls the random process. However, fracture density may vary spatially, so we propose to use a heterogeneous Poisson point process which is more accurate to simulate

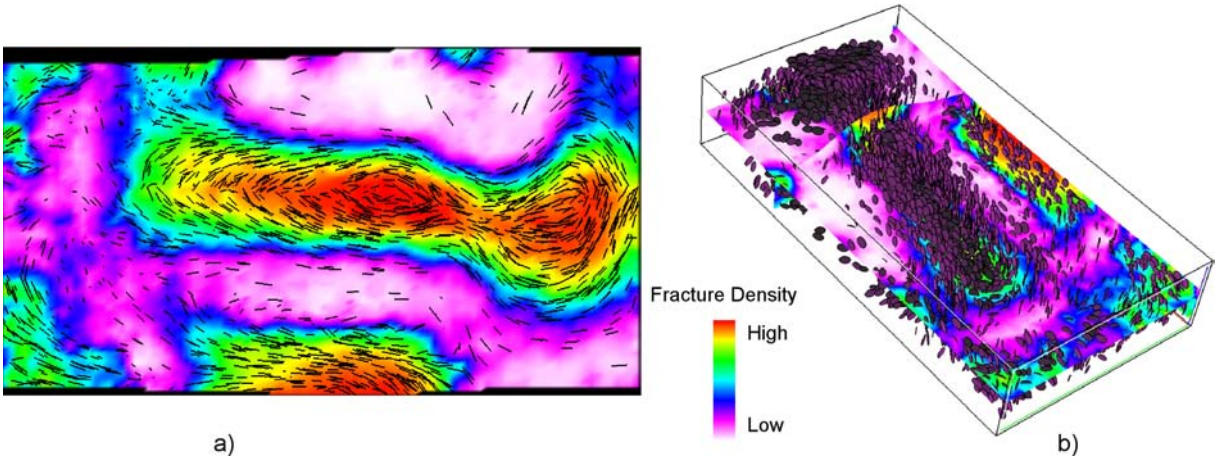

Figure 5: *Simulated DFN, Split Mountain (Utah). a) Top view (fractures are the black lines). b) Side view. In both pictures, the displayed property on cross-sections is the fracture density.*

fracture location (see [15]). A background grid where the local density value is specified, is the modeling support of this stochastic simulation as shown by figure (5).

Fracture orientation

Fracture orientation is simulated from structural analysis information. Fracture orientation highly depends on the type of fracturation: shear, extension and tension fractures (see [11]). So local principal directions of stresses, which are the eigen vectors of the Stress Tensor, are used to constrain the local mean orientation value, as shown by figure (5).

Fracture size

In [3], fracture size is assumed to follow approximately a power law distribution. Moreover, a relationship between fracture size and their spatial position is due to two phenomenon: the presence of an ”inhibition zone” surrounding each fracture during its propagation and the fact that new fractures may be truncated by older ones (see [10]). When DFNs are simulated, these two conditions must be taken into account.

4 Fracture connectivity and equivalent permeability

Once a DFN has been simulated, the equivalent permeability of the fracture network can be assessed. Before computing the equivalent permeability of the media, a preliminary stage is the evaluation of the DFN connectivity. A connectivity graph is built, which nodes correspond to fracture centers and edges are identified to ”pipes”. The conductivity of each pipe is then determined from the fracture permeability and aperture.

Fracture connectivity

Fracture connectivity is a key parameter for estimating the equivalent permeability of the network. Assessing fracture connectivity means computing fracture intersections. However performing intersections between large sets of discrete fractures is computationally intensive. In order to speed-up the computation, an octal tree is built from fracture centers allowing to select the set of neighboring fractures that are likely to intersect another fracture. Several preliminary tests are also made to eliminate as much as possible useless intersection computations. As intersections are computed through our timely optimized

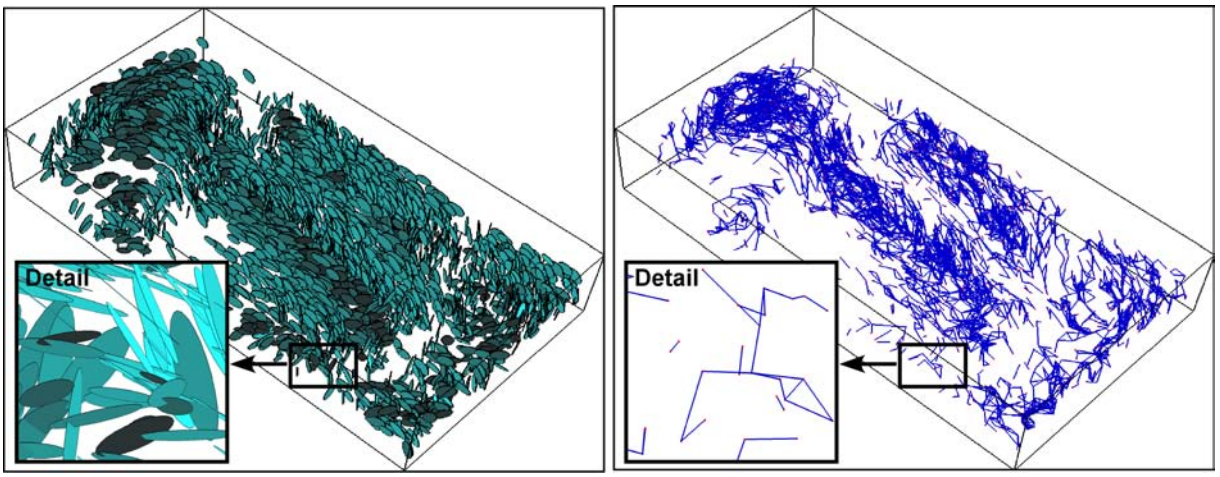

Figure 6: *A discrete fracture network (left) and its connectivity graph (right) (Split Mountain, Utah).*

method, a 3D connectivity graph is built (see figure (6)) storing parameters at its edges. These stored parameters are the relevant geometrical ones relative to the intersection, the transmissivity value determined from the permeability and aperture values of both intersected fractures. This connectivity graph can be used to distinguish subsets of connected fractures. It also enables the assessment of equivalent permeability of DFNs.

Equivalent permeability

Usually the equivalent permeability of DFNs is estimated in each cell of a 3D grid through a permeability tensor integrating fracture connectivity information. The permeability tensor is determined for the grid block flow response to be as close as possible to the fractures response contained in this block.

The size of the grid cell compared to the fracture size is a critical parameter. Below a critical size, fractures can be considered as a rock matrix component; while above it, fractures must be treated as discrete objects influencing the fluid flow. According to the percolation theory in [10] and [16], the impact of the smallest fractures on fluid flow depends on percolation networks. Below a critical fracture density, called the percolation threshold, there are only finite-sized clusters of connected conductors (no percolation), and above the critical density there is an infinite clusters of connected fractures (percolation). Below the critical density value p_c, the fracture density p is linked to a physical property M of the fractured media such as the connectivity or permeability following equation (5).

$$M(p) \sim (p - p_c)^{\tau} \tag{5}$$

τ is a universal scaling exponent, meaning it only depends on the dimension of the percolation model. In [3], Bour has successfully applied the percolation theory to 2D fracture networks presenting a power law length distribution.

Concerning the largest fractures, several pressure gradients can be successively applied to the boundaries of a cell containing a part of these fractures; the flow response of the DFN is then studied at the cell boundaries (see [6] and [14]).

5 Conclusion

The complete workflow of 3D fracture modeling has been investigated in this article. First the focus was the fracture networks characterization integrating geomechanics and data uncertainties to obtain a new fracture parameter, the failure probability, which enables to assess fracture density in case of shear

fractures. A future work will be to take into account tensile fracturation pattern. Then, from fracture density and other fracture characteristics, an object based stochastic simulation has been performed using a heterogeneous Poisson point process to simulate fracture spatial location. Several solutions are still under investigation for simulating fracture size and aperture. Finally, an optimized method for computing 3D fracture networks connectivity has been proposed to assess equivalent permeability of the media.

Acknowledgments

This research work was performed in the frame of the gOcad research project. The companies and universities members of the gOcad consortium are hereby acknowledged. The support of the Carfrac Consortium, and especially IFP, who provided the Split Mountain data set is also gratefully acknowledged.

References

[1] Adler, P. and Thovert, J., (1999). *Fractures and Fracture Networks,* Kluwer Academic Publishers, Dordrecht, 429p.

[2] Blès, J-L. and Feuga, B., (1996). *La Fracturation des Roches,* Editions du B.R.G.M., Orléans, 121p.

[3] Bour, O. and Davy, P., (1997). *Connectivity of random fault networks following a power law fault length distribution,* Water Resources Research, 33, 1567-1583.

[4] Bourne, S., Brauckmann, F., Rijkels, L., Stephenson, B., Weber, A., and Willemse, E., (2000). *Predictive Modelling of Naturally Fractured Reservoirs using Geomechanics and Flow Simulation,* In Proceedings of the 9th ADIPEC.

[5] Goodman, R. E., (1989). *Introduction to Rock Mechanics,* John Wiley & Sons, New York, 576p.

[6] Hartley, J., (1998). *Napsac (release 4.1),* Technical summary document, AEA Technology.

[7] Jaeger, J.C., (1969). *Elasticity, Fracture and Flow, with Engineering and Geological Applications,* 3rd edition Methuen, London, 268p.

[8] Mallet, J.L., (2002). *Geomodeling,* Oxford University Press, New York, 600p.

[9] Mallet, J.L., (2004). *Space-Time Mathematical Framework for Sedimentary Geology,* Mathematical Geology, 36, No.1, 32p.

[10] National Research Council, (1996). *Rock Fractures and Fluid Flow: Contemporary Understanding and Applications,* National Academy Press, Washington D.C., 551p.

[11] Nelson, R.A., (2001). *Geologic Analysis of Naturally Fractured Reservoirs,* Gulf Professional Publishing, 2nd edition, Houston, 320p.

[12] Ouenes, A., (2000). *Practical Application of Fuzzy Logic and Neural Networks to Fractured Reservoir Characterization,* Computer and Geosciences, 26, 953-962.

[13] Ozkaya, S.I., (2002). *CURVAZ - a program to calculate magnitude and direction of maximum structural curvature and fracture-flow index,* Computer and Geosciences, 28, 399-407.

[14] Pouya, A. and Courtois, A., (2002). *Définition de la perméabilité équivalente des massifs fracturés par des méthodes d'homogénéisation,* C. R. Géosciences, 334, 2002, 975-979.

[15] Samantray, A. (1996). *Methodology for Quantifying Subseismic Faults in Petroleum Reservoirs,* PhD thesis, Norwegian University of Science and Technology, Trondheim.

[16] Stauffer, D. and Aharony, A. (1992). *Introduction to the Percolation Theory,* Taylor and Francis, London, 192p.